TÜBİTAK

Turkish Journal of Earth Sciences

http://journals.tubitak.gov.tr/earth/

Research Article

Turkish J Earth Sci
(2014) 23: 427-443
© TÜBİTAK
doi:10.3906/yer-1303-16

Whole-rock geochemistry of basic and intermediate intrusive rocks in the Ishiagu area: further evidence of anorogenic setting of the Lower Benue rift, southeastern Nigeria

Anthony CHUKWU[1,*], Smart CHIKA OBIORA[2]

[1]Department of Geology and Exploration Geophysics, Ebonyi State University, Abakaliki, Nigeria
[2]Department of Geology, University of Nigeria, Nsukka, Nigeria

Received: 29.03.2013 • **Accepted:** 31.03.2014 • **Published Online:** 17.06.2014 • **Printed:** 16.07.2014

Abstract: Petrographic studies on the intrusive rocks from the Ishiagu area show that they are gabbro, dolerites, and diorite. The gabbro and diorite occur as stocks while the dolerites occur as sills in folded sedimentary sequence predominated by shale. Geochemical data confirmed the rocks as basic (gabbro and dolerites) and intermediate (diorite) rocks with silica contents ranging from 42.45 to 50.75 wt.% and 55.03 to 60.24 wt.%, respectively. They are predominantly alkaline (gabbro, dolerites, and diorites) with sparse tholeiites (few gabbro). The basic rocks are made up of calcic plagioclase (An_{49-54}), clinopyroxene, olivine (altered), nepheline, and opaques, while the intermediate rocks consist of plagioclase (An_{41-49}), hornblende, and clinopyroxene. Calcite occurs as a secondary mineral in both groups. Although many samples are moderately to heavily altered (loss on ignition: 2.12–10.46 wt.%), a consistent decrease in magnesium number (Mg#) (gabbro, 0.47; dolerites, 0.37; dolerites, 0.27) and immobile elements (Y, Zr, Hf, Ti, Nb, and Ta), which are more enriched in the intermediate than the basic rocks and similar patterns of spidergrams and rare earth elements (REEs), show that the rocks (gabbro, dolerites, and diorites) are genetically related. The rocks show stronger enrichment in incompatible elements and REEs [$(La/Yb)_n$, 4.83–8.15 for the gabbro, 7.01–7.79 for the dolerites, and 8.85–9.63 for the diorites]. Primitive-mantle normalized trace-element patterns and trace-element ratios of both basic and intermediate rocks indicate similarity to ocean island basalts, which suggests a garnet-lherzolite mantle source. The ratios of La/Nb, Th/La, and Th/Nb and the high ratio of Nb/La (1.18–1.50 for gabbro, 1.37–1.95 for dolerites, and 1.21–1.32 for diorites) indicate a high $^{238}U/^{204}Pb$ (HIMU) mantle source region. There is no evidence of significant crustal contamination on the basic and intermediate rocks, which may be related to the rapid ascent of the magmas in an intracontinental rift setting similar to the East African rift.

Key words: Intrusive rocks, alkaline affinity, HIMU mantle source, intracontinental rift setting, Ishiagu area, Lower Benue rift, Nigeria

1. Introduction

The Lower Benue rift is the southern part of the intracontinental Benue rift-basin, which extends from the Niger Delta northeast towards the southern part of Cameroun, a distance of about 1000 km long and 80 km wide. Its evolutionary history was traced to the opening of the Gulf of Guinea and the South Atlantic during the separation of the South American plate from the African plate in the Mesozoic era (Burke et al., 1971; Grant, 1971) (Figure 1), accompanied by magmatic activities that span the Jurassic (Bajocian) to the Tertiary (Umeji, 2000).

The first report of the existence of intrusive rocks in the Lower Benue rift was by Wilson and Bain (1928), who described the rocks exposed at Lokpanta during the construction of the Port Harcourt–Enugu railway line as intrusions (Obiora and Charan, 2010). The intrusive and volcanic rocks in the Lower Benue rift have been described as intermediate to basic in composition and associated with lead-zinc mineralization (Farrington, 1952; Gunthert and Richards, 1960; Cratchley and Jones, 1965; Nwachukwu, 1972), as cited by Obiora and Charan (2010).

Burke et al. (1971) described the rocks (volcanic and intrusive) around the Abakaliki area (Figure 1) as andesite lavas and tuffs and proposed a subduction origin for the rocks in the Benue rift. However, Olade (1978, 1979) reported alkali basalts and tuffs with spilite using petrographic and geochemical data and concluded that the rocks were within plate 'hotspot' basalts. Some others (Benkhelil, 1986; Maluski et al., 1995; Obiora and Umeji, 1995, 1997, 2004; Obiora, 2002) suggested a predominantly alkaline character for gabbro, monzonite, diorite, syenite, basalts, and trachytes in the lower Benue rift, reflecting an extensional and within-plate setting. In addition to the predominant alkaline affinity for the intrusive and volcanic rocks in the lower Benue rift, Coulon et al. (1996)

* Correspondence: tonaro4u@yahoo.com

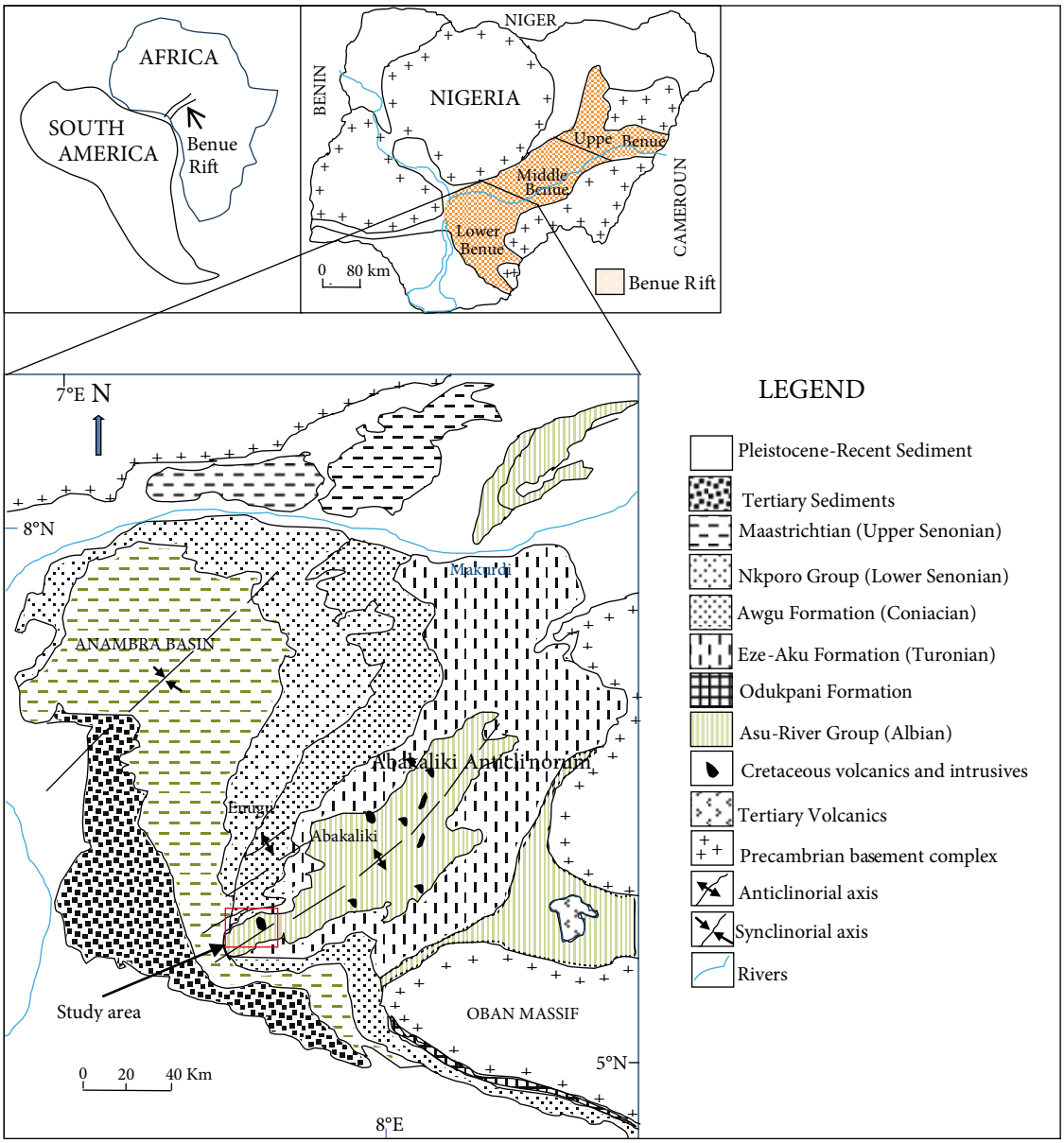

Figure 1. Geological map of Lower Benue rift and its position relative to Nigeria and Africa.

and Obiora and Charan (2010, 2011a) suggested a high $^{238}U/^{204}Pb$ (HIMU) mantle source region for these rocks.

Generally, the intrusive rocks along the Ishiagu axis (Figure 1) in the Lower Benue rift have been relatively scarcely studied in detail. Apart from the intrusive exposure described in Eziator (boundary between Ishiagu and Awgu, Enugu State) by Gunthert and Richards (1960), Obiora (2002), and Obiora and Charan (2010), there have been no detailed studies on the geochemistry of the intrusive rocks in the Ishiagu area.

This paper presents whole-rock major and trace element data of basic to intermediate intrusive rocks in the Ishiagu area, petrogenic interpretations, and further characterization of the tectonic setting of the Lower Benue rift.

1.1. Geological setting and local geology

The Benue rift, the failed arm of the triple junction, was formed during the separation of the South American plate from the African plate in the Mesozoic times through the Gulf of Guinea-South Atlantic-Benue triple junction (Burke et al., 1971; Grant 1971), as cited by Obiora and Charan (2011a) (Figure 1).The Benue rift is subdivided into Upper, Middle, and Lower parts based on geographic locations (Petters, 1978; Nwajide, 1990; Idowu and Ekweozor, 1993; Obaje et al., 1999) (Figure 1). The Benue rift basin is filled mainly by Pre-Santonian (Late

Aptian to Coniacian) sedimentary rocks that have been compressionally folded, faulted, and uplifted in several places and have undergone regional burial metamorphism at the anchizonal to lower greenschist grade (Benkhelil, 1986, 1987; Obiora, 2002; Obiora and Umeji, 2004; Obiora and Charan, 2011b). The mechanism of triple junction rifting involves mantle plume, crustal stretching and thinning, block faulting, and igneous activities (Olade, 1975; Bott, 1976). However, other theories were proposed, such as the transform fault mechanism along the northern margin of the Gulf of Guinea (Benkehlil, 1986) and the membrane stress model, which explains the presence of a series of anticlinorium and synclinorium suggesting a deformational stage in the evolution of the rift (Obiora and Charan, 2011a). Farrington (1952) and Burke et al. (1971, 1972) proposed a subduction origin for the Benue rift igneous suite due to existence of folds and a wrong interpretation of the pyroclastic rocks in the Abakaliki area as andesite. However, Obiora and Charan (2010) further supported an extensional origin rather than collision. The intrusive bodies intruded the folded sedimentary sequence, which is constituted predominantly of shale and subordinate alternating shales, sandy-shales, siltstones, and mudstones of the Late Aptian to Albian locally known as the Asu River Group. On the whole, 11 intrusive bodies were studied, as shown in Figure 2, with detailed description of their locations given in Table 1. The intrusives are grouped into 3 categories based on their modal and textural characteristics, namely 7 gabbro intrusive bodies, 3 dolerite intrusive bodies, and 1 diorite intrusive body. The gabbro and diorite occur as stocks while the dolerites occur mostly as sills. Generally, the stocks have 10–350 m width, 400–600 m length, and 10–60 m height while the sills have 50–200 m width, 200–400 m length, and 50 m height. The sills have an orientation trending northeast–southwest. The contacts of the intrusives with the host rock (mainly shale) are generally sharp, although baking of the host rocks at the contacts is mild, especially where exposed by quarry activities (locations 1, 6, 8, and 9). Since the age of the host rocks (shale, siltstone, and mudrocks) is Albian (Benkhelil, 1986, 1987), the intrusives are probably of post-Albian age. In support of the post-Albian, Umeji

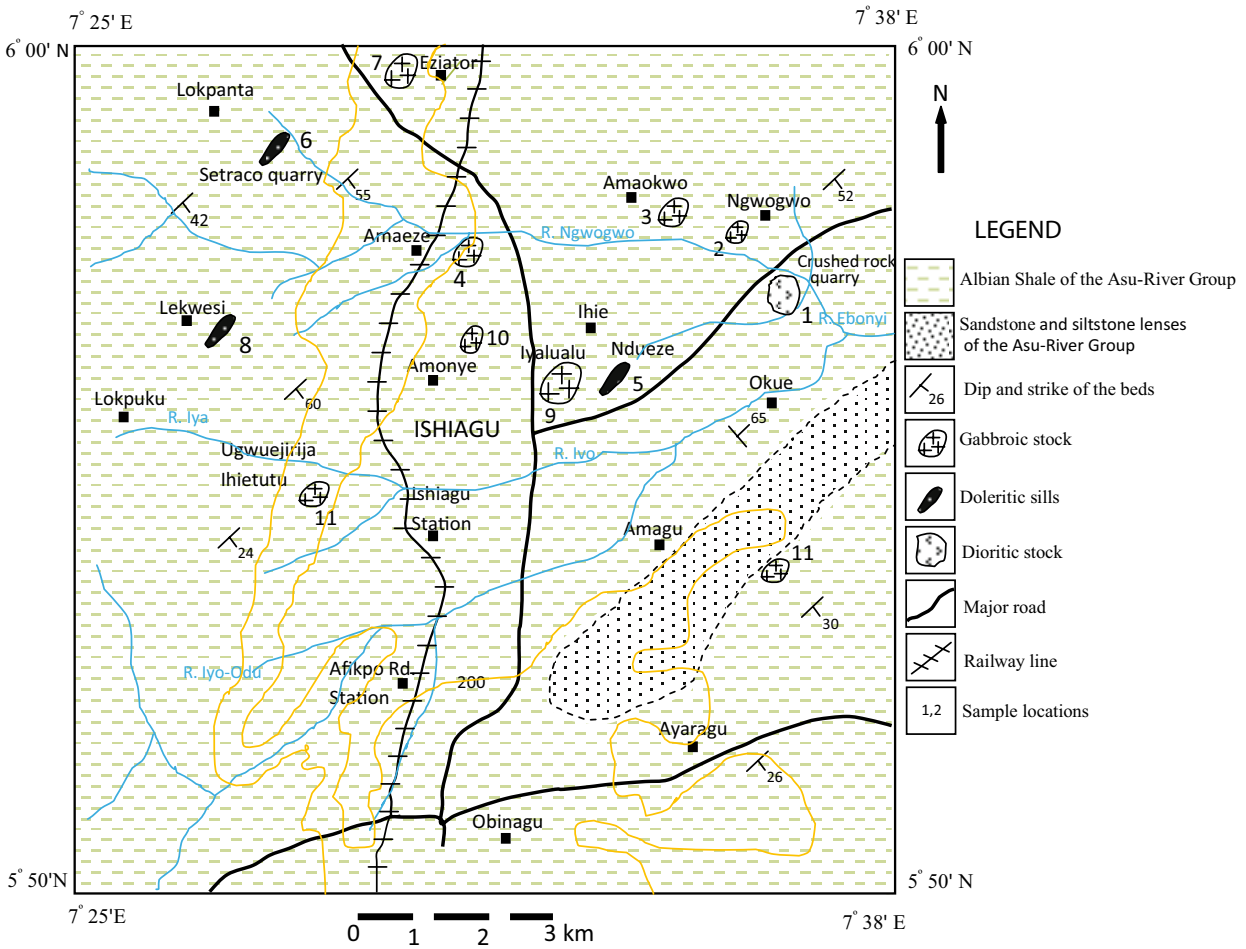

Figure 2. The geological map of Ishiagu and environs, southeastern Nigeria, showing the locations of the studied intrusive rocks.

Table 1. Details of the locations of samples of the intrusive rocks in the Ishiagu area.

Sample no.	Location no. (Figure 2)	Long. and lat.	Location name	Name of rock
CA01A	1	07°34′36.4″E 05°57′16.4″N	Crushed Rock Ind. (medium part)	Diorite
CA01B		07°34.822′E 05°57.232′N	Amaokwe extension of crushed rock	Diorite
CA01C			Crushed Rock Ind. (coarse part)	Diorite
CA01D			Okue extension of crushed rock	Diorite
CA01E			Ngwogwo extension of crushed rock	Diorite
CA01F		07°34′36.4″E 05°57′16.4″N	Crushed Rock Ind. (fine part)	Diorite
CA02	2	07°34.396′E 05°57.454′N	Ngwogwo Amadin	Gabbro
CA03	3	07°34′24.9″E 05°57′37.4″N	Ngwogwo Onuagbo - 1	Gabbro
CA03B		Similar	Ngwogwo Onuagbo - 2	Gabbro
CA04	4	07°33′00.2″E 05° 57′44.2″N	Obu-Ugwu Amaeze	Gabbro
CA06	5	07°33′43.2″E 05°56′57.2″N	Ndueze Ihie	Dolerite
CA08	6	07°29′44.6″E 05°58′21.3″N	Setraco Quarry Amaeze - 1	Dolerite
CA08B			Setraco Quarry Amaeze - 2	Dolerite
CA09	7	07°31.939′E 05°59.867′N	Eziator (fine part)	Gabbro
CA09A			Eziator (coarse part)	Gabbro
CA10	8	07°28.864′E 05°56.888′N	Crushed Stone Lekwesi	Dolerite
CA11B	9	07°33′32.4″E 05°56′51.9″N	Iyalualu Ihie (fine part)	Gabbro
CA11C		07°33.553′E 05°56.902′N	Iyalualu Ihie (coarse part)	Gabbro
CA12	10	07°33′19.7″E 05°56′48.4″N	Amanhoho Amonye	Gabbro
CA13	11	07°33′30.8″E 05°54′25.6″N	Amagu	Gabbro

(2000) reported that the intrusives in the Lower Benue rift are Cretaceous.

2. Analytical methods

The representative rock samples were collected during field work for petrographic and whole-rock geochemical analyses. Thin sections used for the petrographic studies were prepared at the Thin Section Laboratory of the Department of Earth Sciences, Kogi State University, Anyigba, Nigeria. The freshest 20 samples were pulverized at the geochemical laboratory in the Department of Geology, University of Nigeria, Nsukka, Nigeria. A diamond crusher machine and agate mortar were used for pulverizing. The analyses were performed by inductively coupled plasma mass spectrometry at Activation Laboratories, Ontario, Canada, for major- and trace-element analyses. The open-acid digestion method outlined by Roy et al. (2007) was adopted for sample preparation. First, 50 mg of the sample powder was weighed and 10 mL of acid mixture (210 mL of HF, 90 mL of HNO_3, and 30 mL of $HClO_4$) was added

to each sample in the ratio of 7:3:1. The solution was thereafter heated on a hot plate (~150 °C) for up to 1 h to liberate the gases to form a crystal paste. Thereafter, 20 mL of 1:1 HNO_3 and distilled water was added and warmed (~70 °C) to dissolve the precipitate, after which 5 mL of 1 ppm ^{103}Rh was added as an internal indicator/standard. The detection limits of the elements analyzed are given in Figure 2. They range as follow: major oxides, 0.001–0.01 wt.%; trace elements, 0.1–30 ppm; and rare earth elements (REEs), 0.04–0.10 ppm. The standards used were DH-1a, NIST 694, DNC-1, GBW 07113, LKSD-3, TDB-1, W-2a, DTS-2b, SY-4, CTA-AC-1, BIR-1a, NCS DCN 86312, ZW-C, NCS DC 70014, NCS DC 86316, NCS DC 70009 (GBW07241), 0REAS 100a (Fusion), OREAS 101a (Fusion), JR-1, NCSDC 86318, SARM3, USZ 25-2006 and USZ 42-2006 (for more details, see http://www.actlabs.com).

3. Results

3.1. Field and petrographic characteristics of the intrusive rocks

The stocks and sills constitute small hills within the generally flat sedimentary terrain in the study area. The subdivision of the intrusives into gabbro (locations 2, 3, 4, 7, 9, 10, 11), dolerite (locations 5, 6, 8), and diorite (location 1) is based on the mineralogy and textural appearances from thin section. The gabbroic rocks are medium- to coarse-grained, mesocratic to melanocratic, and show ophitic to subophitic textures (Figures 3a and 3b). Large crystals of clinopyroxenes, (8.38 mm) completely enclose laths of plagioclase (1.83 mm). The minerals include clinopyroxene (augite) (19%–49%), plagioclase (An_{43-52} calcic andesine-labradorite) (46%–69%), altered olivine (4%–8%), nepheline (1%–3%), and opaques (1%–6%) (Figure 3). Calcite and chlorite crystals occur as secondary minerals from the alteration of clinopyroxene. The dolerites have similar characteristics as the gabbro; the major difference is in their textures. The dolerites are medium-grained and melanocratic with subophitic textures (Figure 3c). The mineral constituents are clinopyroxene (augite) (26%–31.5%), laths of randomly oriented plagioclase (An_{54}, labradorite) (57%–68%), and opaques (magnetite and ilmenite) (4%–7.5%). Calcite, sericite, and chlorite occur as alteration products. The plagioclase is sericitized. The dioritic rocks are medium- to coarse-grained and leucocratic to mesocratic, with subophitic textures. The mineral constituents are plagioclase (64.5%–71%) of andesine composition (An_{49}), hornblende (10%–18%), clinopyroxene (11%–22%) (augite), and opaques (1%–4%). Biotite (1%–3%) is accessory while quartz is interstitial. Calcite (2%) and sericites occur as secondary minerals and alteration products of pyroxene and plagioclase. The presence of calcites and other alteration minerals that are higher in the gabbro and dolerites can be attributed to the effect of saline water, which was reported to have existed in the past in the area (Umeji, 2000).

3.2. Whole-rock geochemistry

The major oxides and trace and REE data of the studied intrusive rocks are presented in Table 2. The basic rocks (gabbro and dolerites) have SiO_2 contents ranging from 42.45 to 50.75 wt.%, whereas the intermediate rocks (dioritic stock) have 45.77–61.47 wt.% SiO_2. Loss on ignition (LOI) of the intrusives is generally high, and particularly that of the dolerites and the gabbro, which have 4.60–9.28 wt.% and 2.21–10.46 wt.%, respectively. However, the diorite stocks have relatively moderate values of 1.06–3.44 wt.%. The wide variation in the LOI of the intrusives attests to the alteration and probable elemental mobility of the intrusives, which reflect contributions by secondary hydration.

3.3. Chemical classification and nomenclature of the rock

The intrusive rocks can be grouped into intermediate (diorites) and basic (dolerites and gabbro) rocks based on their silica contents (Table 2). In Figure 4, in the Zr/Ti versus Nb/Y diagram of Winchester and Floyd (1977) with fields as modified by Pearce (1996), the gabbroic and doleritic rocks predominantly plot within the alkali basalt field while the dioritic rocks plot mainly in the trachyandesite field. Samples CA09A and CA09 of the gabbro from the Eziator plot in the subalkaline (tholeiite) section of the diagram. The intrusives have moderate to low MgO from the basic to the intermediate rocks. This is reflected in the Mg numbers (Mg# = $Mg/Mg^{2+}+Fe^{2+}$ in moles), which range from 0.39 to 0.52 (average: 0.42) in gabbro, 0.30 to 0.50 (average: 0.37) in dolerites, and 0.19 to 0.40 (average: 0.27) in diorites. Such values indicate that the intrusives do not represent primary melts and may have experienced some degree of olivine and clinopyroxene fractionation from the primary magma.

3.4. Multielement diagrams

The spider diagrams are presented in Figure 5a–5c. They consist of concentrations of the incompatible trace elements and selected REEs, normalized to the values of primitive mantle after Sun and McDonough (1989). Generally, the patterns show enrichments in the incompatible trace elements that are characteristic of ocean island basalt (OIB) (Figure 5). The patterns of the gabbro and dolerite samples (Figures 5a and 5b) look similar in their elemental distribution. Both rock samples (gabbro and dolerite) show relative enrichment in Ba; 3 samples are depleted in Rb and K and 1 sample of the gabbro is depleted in Sr. In contrast, the dioritic rock samples are depleted in Sr, P, and Ti, except for 1 sample (CA01C), which has a similar pattern as the gabbro and dolerites (Figure 5c). The Ba, Rb, and K anomalies in the gabbro and dolerite samples

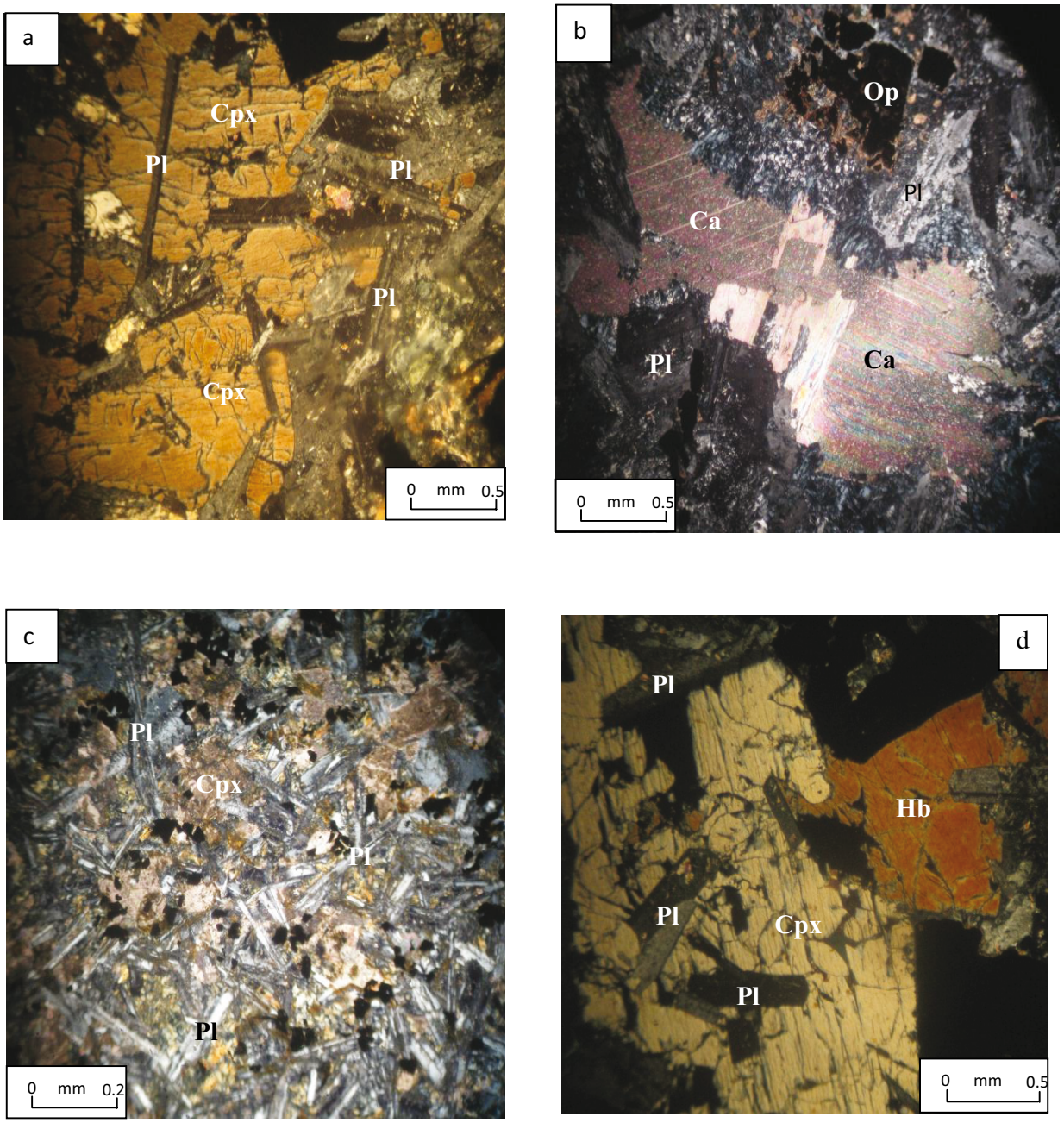

Figure 3. Photomicrograph of the intrusives showing: **(a)** large crystal of clinopyroxene (Cpx) in an ophitic relationship with long crystals of plagioclase (Pl) in the gabbro, cross-polarized light (X4); **(b)** crystals of plagioclase (Pl), calcite (Ca), and opaque minerals (OP) replacing clinopyroxenes in the gabbro, cross-polarized light (X4); **(c)** doleritic texture [random orientation of plagioclase (Pl) laths] in the dolerite, cross-polarized light (X4); **(d)** plagioclase (Pl) in an ophitic relationship with the clinopyroxene (Cpx) and hornblende (Hb) in the diorites, cross-polarized light (X4).

can be attributed to the alteration effects of the rocks while the depletion of Sr, P, and Ti in the diorites indicates substantial fractionation of plagioclase, apatite, and Fe-Ti oxides (magnetite and ilmenite), respectively, from the melt. The absence of Nb-Ta anomaly strongly indicates an anorogenic rift environment for the rocks.

3.5. REE patterns

The REEs (Table 2) were normalized using values from Sun and McDonough (1989). The chondrite-normalized REE patterns for the rocks are presented in Figure 6. The patterns are similar for the gabbro, dolerites, and diorites, implying a common origin. They generally show

Table 2. Major oxides (wt.%), trace elements (ppm), and rare earth elements (ppm) analysis of the Ishiagu intrusive rocks. Dl = detection limit.

	Diorites						Dolerites			
	CA01A	CA01B	CA01C	CA01D	CA01E	CA01F	CA06	CA08	CA08B	CA10
SiO_2	55.03	60.25	45.77	61.47	60.24	56.7	42.5	43.4	48.64	44.66
TiO_2	1.88	1.313	3.955	1.034	1.256	1.522	4.62	3.53	4.424	2.986
Al_2O_3	15.12	15.43	14.98	15.01	15.52	15.26	14.8	14.1	15.64	14.08
Fe_2O_3(t)	9.64	7.72	12.33	6.55	7.55	8.25	13.6	13.6	15.19	12.39
MnO	0.171	0.147	0.15	0.129	0.151	0.153	0.15	0.17	0.092	0.195
MgO	2.21	1.32	4.59	0.84	1.24	1.58	7.62	3.28	4.54	3.24
CaO	4.7	3.28	8.5	2.53	2.83	4.07	8.45	9.48	1.22	9.52
Na_2O	5.31	5.95	3.91	5.65	5.99	5.54	3.1	3.06	4.67	2.57
K_2O	2.15	2.8	0.96	3.14	2.92	2.45	0.24	0.93	0.08	0.19
P_2O_5	0.62	0.35	0.55	0.24	0.34	0.45	0.45	0.86	0.73	0.95
LOI	2.12	1.06	3.44	3.35	1.25	1.99	4.6	7.47	4.61	9.28
TOTAL	98.96	99.63	99.14	99.95	99.28	97.97	100	99.8	99.82	100
Na_2O+K_2O	7.46	8.75	4.87	8.79	8.91	7.99	3.34	3.99	4.75	2.76
Sc	10	8	20	6	8	9	16	17	18	13
Be	3	4	<1	5	5	4	1	2	<1	2
V	81	29	247	20	29	44	252	227	287	152
Cr	50	70	60	180	140	110	180	40	50	30
Co	13	6	31	5	6	8	52	36	89	22
Ni	240	310	240	940	690	550	330	200	260	170
Cu	<10	<10	40	<10	<10	<10	30	20	20	<10
Zn	130	130	110	120	130	110	120	150	120	270
Ga	28	30	22	30	29	28	22	25	28	25
Rb	39	48	19	57	51	45	5	13	<2	3
Sr	494	243	1167	413	443	442	700	591	499	584
Y	48	57	29	53	58	53	24	38	25	41
Zr	543	695	250	734	743	629	238	367	316	413
Nb	71	81	37	78	78	76	30	47	42	53
Mo	2	6	<2	5	6	4	<2	3	<2	3
Ag	1.9	5.4	2	5.6	5.6	4.8	1.8	2.7	2.2	3
Sn	5	8	3	9	9	7	3	4	4	3
Cs	<0.5	<0.5	<0.5	<0.5	<0.5	<0.5	0.8	0.9	<0.5	2.5
Ba	481	507	627	580	599	486	213	552	83	206
Hf	11.4	15.4	5.9	15.4	16.4	14.2	5.5	8.1	6.9	8.9
Ta	4.6	5.3	2.6	5.1	5.2	4.9	2.2	3.2	2.9	3.5
W	<1	1	<1	3	1	1	<1	<1	<1	<1
Pb	<5	<5	<5	8	<5	<5	<5	<5	<5	9
Th	6.1	8.4	2.6	8.7	8.8	7.9	2.1	3	2.3	3.3
U	1.8	2.5	0.8	2.6	2.7	2.4	0.7	1	0.5	1.1
La/Nb	0.76	0.82	0.81	0.79	0.82	0.82	0.71	0.73	0.51	0.71
Th/Nb	0.086	0.1	0.07	0.11	0.11	0.1	0.07	0.06	0.05	0.06
Th/La	0.11	0.13	0.09	0.14	0.14	0.13	0.1	0.09	0.11	0.09

Table 2. (continued).

	Gabbro										
	CA02	CA03	CA03B	CA04	CA09	CA9A	CA11B	CA11C	CA12	CA13	Dl
SiO_2	46.09	48.04	46.91	45.22	50.75	47.32	45.77	47.01	46.81	44.42	0.01
TiO_2	4.662	3.663	4.146	4.263	2.316	1.872	4.516	3.904	3.484	4.001	0.001
Al_2O_3	15.02	15.76	14.69	16.05	13.26	13.18	15.17	15.27	16.82	14.53	0.01
Fe_2O_3(t)	12.08	11.16	12.48	12.27	10.58	9.53	12.58	12.59	10.5	13.31	0.01
MnO	0.146	0.144	0.163	0.144	0.149	0.122	0.149	0.158	0.13	0.156	0.001
MgO	4.98	4.42	4.62	4.39	6.36	3.83	4.73	4.56	3.79	7.52	0.01
CaO	8.54	7.75	7.95	9.13	4.81	10.7	7.92	8.8	8.53	6.79	0.01
Na_2O	3.25	4.12	4.04	3.91	5.32	2.3	3.27	3.83	3.6	3.73	0.01
K_2O	1.38	1.55	1	1.1	0.05	0.13	1.42	1.11	1.81	0.37	0.01
P_2O_5	0.58	0.63	0.59	0.49	0.29	0.21	0.61	0.56	0.47	0.5	0.01
LOI	3.22	3.22	2.7	3.44	4.94	10.46	2.53	2.21	2.27	4.41	--
TOTAL	99.95	100.5	99.31	100.4	98.82	99.65	98.66	99.99	99.75	100.4	--
Na_2O+K_2O	4.63	5.67	5.04	5.01	5.37	2.43	4.69	4.94	5.41	4.1	
Sc	20	19	20	20	23	24	18	23	19	17	1
Be	1	1	1	1	<1	1	1	1	1	1	1
V	258	224	253	280	190	176	260	282	237	252	5
Cr	110	70	40	80	150	230	80	30	30	210	20
Co	32	27	31	31	29	31	34	33	26	48	1
Ni	440	350	160	410	270	390	280	200	190	420	20
Cu	30	30	30	50	60	50	30	40	50	30	10
Zn	110	100	120	100	80	50	120	110	90	120	30
Ga	22	22	23	22	20	18	23	24	24	21	1
Rb	22	30	13	24	<2	4	23	21	38	10	2
Sr	731	1274	735	617	106	256	745	721	892	571	2
Y	30	34	34	26	22	71	29	30	27	25	2
Zr	289	317	326	256	162	124	299	302	281	241	4
Nb	39	40	41	34	16	12	40	36	34	30	1
Mo	<2	2	<2	<2	<2	<2	2	<2	<2	<2	2
Ag	2.1	2.4	2.5	1.7	1.2	<0.5	2.2	2.1	2	1.7	0.5
Sn	4	3	4	3	3	2	4	3	3	3	1
Cs	<0.5	<0.5	<0.5	0.6	<0.5	1.4	0.6	0.5	0.9	1.2	0.5
Ba	878	1216	532	322	68	206	939	440	570	178	3
Hf	6.5	7.3	7.3	5.9	2.8	8.9	6.8	6.8	6.3	5.6	0.2
Ta	2.7	2.7	2.8	2.3	1	0.8	2.9	2.5	2.4	2.2	0.1
W	<1	<1	<1	2	<1	<1	<1	<1	<1	<1	1
Pb	<5	<5	<5	<5	<5	9	<5	<5	<5	<5	5
Th	2.4	2.7	2.6	2	1.6	1.2	2.5	2.5	3	2	0.1
U	0.8	0.8	0.8	0.6	0.5	0.3	0.8	0.8	0.8	0.7	0.1
La/Nb	0.67	0.76	0.7	0.68	0.85	0.84	0.67	0.71	0.74	0.73	
Th/Nb	0.06	0.07	0.06	0.06	0.1	0.1	0.06	0.06	0.09	0.07	
Th/La	0.09	0.09	0.09	0.09	0.12	0.12	0.09	0.1	0.12	0.09	

Table 2. (continued).

	CA01A	CA01B	CA01C	CA01D	CA01E	CA01F	CA06	CA08	CA08B	CA10
La	53.7	66.1	30.1	61.7	64.3	62.2	21.2	34.2	21.5	37.5
Ce	121	143	67.4	135	141	136	51	82	53.2	90.6
Pr	14.3	16.5	8.54	15.7	16.4	16.5	6.66	10.7	7.08	11.9
Nd	60.8	68.1	38.4	63	69.8	67.7	30.9	50.3	32.2	55.8
Sm	13.4	14.9	8.7	14	15.3	15.2	7.7	12.2	7.9	13.4
Eu	4.09	4.19	3.06	3.55	4.16	4.28	2.45	3.85	2.12	4.24
Gd	12.3	13.7	8.8	12.5	13.8	14.1	7	11.7	7.5	12.1
Tb	1.9	2.2	1.3	2.1	2.2	2.2	1	1.7	1.1	1.8
Dy	9.9	11.4	6.5	10.8	11.7	11.6	5.3	8.3	5.5	8.8
Ho	1.8	2.2	1.2	2.1	2.3	2.1	1	1.5	1	1.6
Er	4.8	5.7	3.1	5.5	5.9	5.7	2.4	3.8	2.7	4.2
Tm	0.66	0.82	0.4	0.8	0.84	0.83	0.32	0.51	0.36	0.56
Yb	4	5.3	2.4	5	5.2	5	2	3.1	2.2	3.3
Lu	0.62	0.77	0.35	0.76	0.75	0.73	0.3	0.46	0.33	0.49
∑REE	299.18	350.69	177.2	329	349.49	339.9	136.8	220.5	142.57	242.05
∑LREE/ ∑HREE	7.32	7.33	6.37	7.32	7.19	7.04	6.08	6.1	5.89	6.37
La_n/Yb_n	9.63	8.94	8.99	8.85	8.87	8.92	7.61	7.91	7.01	8.15
Tb_n/Yb_n	2.16	1.89	3.36	1.91	1.92	1.9	2.27	2.49	2.43	2.48
Dy/Yb	2.48	2.15	2.71	2.16	2.25	2.32	2.65	2.68	2.5	2.67
Eu/Eu*	0.99	0.91	1.07	0.82	0.87	0.89	1.03	0.99	0.85	1.02

Table 2. (continued).

	CA02	CA03	CA03B	CA04	CA09	CA9A	CA11B	CA11C	CA12	CA13	Dl
La	26	30.4	28.7	23.1	13.6	10.1	26.9	25.4	25.2	22	0.1
Ce	61	71.2	67.7	53.8	30.2	23.8	64.7	60.4	59.8	52.6	0.1
Pr	8.16	9.53	8.8	7.21	3.83	3.03	8.36	8	7.69	6.92	0.05
Nd	38.3	42.9	41.9	34.3	19.1	13.3	38.9	37.4	35.5	32.1	0.1
Sm	9.5	10.4	10.1	8.8	5.3	4.1	9.4	9	8.7	8.1	0.1
Eu	3.15	3.47	3.31	2.93	1.95	1.38	3.06	3	2.79	2.68	0.05
Gd	8.8	10	10.2	7.9	5.9	4.3	8.7	8.6	7.8	7.4	0.1
Tb	1.3	1.5	1.4	1.2	0.9	0.7	1.3	1.3	1.3	1.1	0.1
Dy	6.6	7.7	7.4	6.1	4.7	3.6	6.7	6.8	6.1	5.6	0.1
Ho	1.2	1.4	1.4	1.1	0.8	0.7	1.2	1.2	1.1	1	0.1
Er	3	3.5	3.5	2.8	2.2	1.8	3.2	3	2.7	2.5	0.1
Tm	0.41	0.48	0.46	0.37	0.3	0.25	0.43	0.41	0.39	0.35	0.05
Yb	2.4	2.8	2.8	2.2	1.9	1.5	2.6	2.5	2.4	2.1	0.1
Lu	0.37	0.43	0.41	0.35	0.29	0.21	0.39	0.37	0.34	0.33	0.04
∑ REE	167.04	192.2	184.8	149.2	89.02	67.39	172.78	164.38	159.02	142.1	
∑LREE/ ∑HREE	5.94	5.91	5.7	5.78	4.24	4.16	6.05	5.8	6.19	5.97	
La_n/Yb_n	7.77	7.79	7.35	7.53	5.13	4.83	7.42	7.29	7.53	7.52	
Tb_n/Yb_n	2.46	2.44	2.27	2.48	2.15	2.12	2.27	2.36	2.46	2.38	
Dy/Yb	2.75	2.75	2.64	2.77	2.47	2.4	2.58	2.72	2.54	2.67	
Eu/Eu*	1.06	1.05	1	1.08	1.07	1.01	1.04	1.05	1.04	1.06	

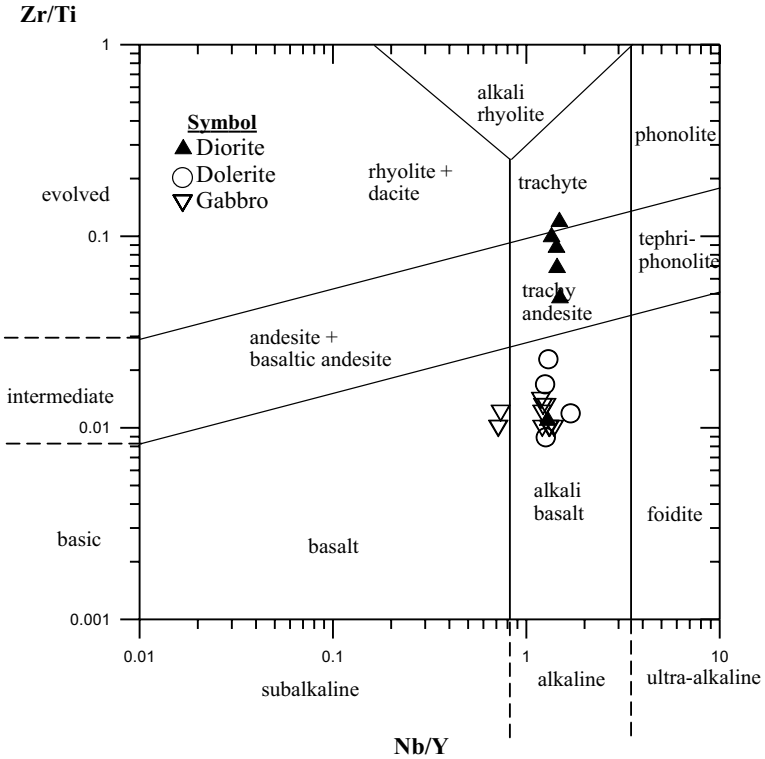

Figure 4. Plot of Zr/Ti vs. Nb/Y diagram of Winchester and Floyd (1977) with fields as modified by Pearce (1996) for the discrimination of different magma series and their differential products. Unfilled triangles = gabbro, unfilled circles = dolerites, filled triangles = diorites.

enrichment in the light REEs (LREEs) relative to the heavy REEs (HREEs). The enrichment in the LREEs is a characteristic of OIB (Figure 6) and shows the presence of residual garnet in the source.

The ratios of LREEs to HREEs of the intrusives (approximately 5–8 in the gabbro, 7–8 in the dolerites, and 9–10 in the diorites) are moderately enriched. This is reflected in the values of $(La/Yb)_n$, which range from 5 to 8 in the gabbro, 7 to 8 in the dolerites, and 9 to 10 in the diorites approximately. Eu/Eu* values for the intrusives generally range from 0.82 to 1.07 (gabbro: 1.00–1.08, dolerites: 0.85–1.03, and diorites: 0.82–1.07) (Table 2); this indicates the absence of positive/negative Eu-anomaly in the rock samples, except for 1 dioritic sample that shows mild negative anomaly (Eu/Eu* value of 0.82, approximately 0.8). This is consistent with the absence of negative Eu-anomaly in the REE patterns (Figure 6) with the exception of 1 dioritic rock sample, in which mild negative anomaly reflects fractionation of feldspars from the melt.

4. Discussion

4.1. Possible alterations of the rocks

It is generally reported that igneous rocks with LOI of greater than 2 wt.% are regarded as altered (e.g., Burianek et al., 2008). Hence, the studied rocks have undergone some degree of alteration, with the gabbro having the highest alteration LOI (2.21–10.46), followed by the dolerites (LOI: 4.60–9.28) and then the dioritic rock, with only 3 samples altered (LOI: 2.12–3.44). This is supported by the greater contents of well-developed calcite crystals along with ilmenite as a result of the breakdown of the clinopyroxene in the basic rocks relative to the dioritic rocks. The involvement of a fluid phase may have caused the depletion and enrichment of some elements in the spider diagrams of the studied rocks. The depletions in the large-ion lithophile elements (Ba, Rb, and K) in Figure 5 could be attributed to the presence of an aqueous fluid phase, which is commonly concentrated in the continental crust (Rollinson, 1993).

4.2. Magma source region

The ratio of La/Ta (7.41–13.60) of the studied rocks indicates an asthenospheric mantle source (Table 3). According to Fitton et al. (1988), Leat et al. (1988), and Thompson and Morrison (1988), La/Ta ratios have been used to distinguish between asthenospheric magma sources for rift-related environments and an index of crustal contamination. Leat et al. (1988) suggested that rocks with La/Ta ratios of <22 are derived from an

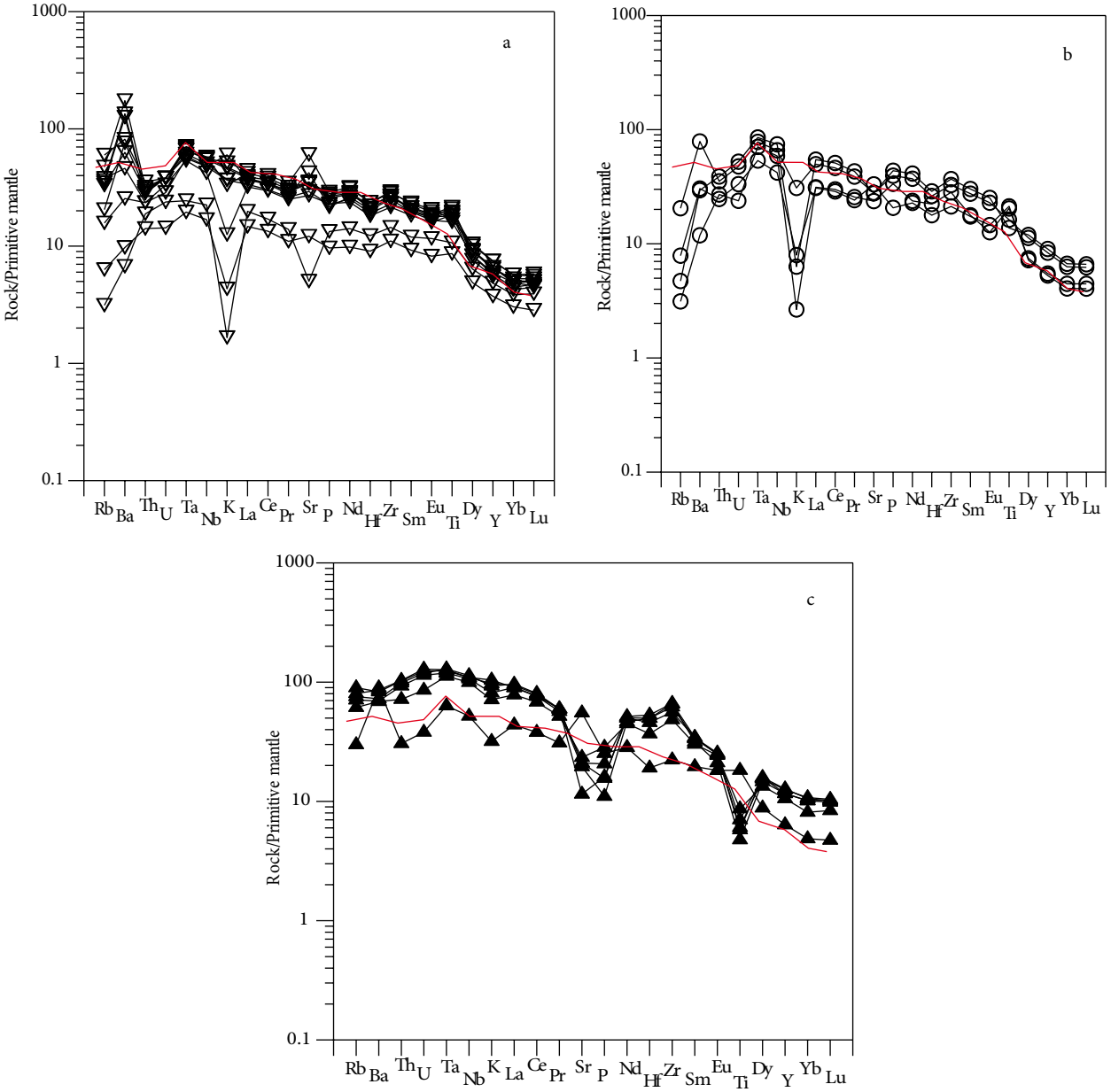

Figure 5. Primitive mantle normalized spider diagrams of **(a)** diorites, **(b)** dolerites, and **(c)** gabbro, similar to the OIB pattern of Sun and McDonough (1989) (red line). Symbols as in Figure 4.

asthenospheric source, whereas Thompson and Morrison (1988) proposed that La/Ta ratios between 10 and 12 originate from an asthenospheric source while values of >30 indicate crustal contamination. The presence of garnet as a residual phase in the melt source region is inferred from the $(Tb/Yb)_n$ ratio (Sayıt and Göncüoglu, 2009). The enrichment in LREEs relative to HREEs in the intrusives, which is reflected in the low $(Tb/Yb)_n$ ratios (2.12–2.48 in gabbro, 2.27–2.49 in dolerites, and 1.89–3.36 in diorites), indicates a garnet-bearing source. The Dy/Yb ratios, which range from 2.40 to 2.77 in gabbro, 2.5 to 2.68 in dolerites, and 2.15 to 2.48 in diorites, also suggest a garnet-bearing lherzolite source (Sayıt and Göncüoglu, 2009). According to Kearey and Vine (1990), the upper mantle has the composition of peridotite, containing abundant olivine and less than 15% garnet. Garnet in the residual melt suggests a depth of at least 80 km (Wilson, 1989), which indicates that the magma generation should have occurred within the asthenosphere.

The presence of garnet in the mantle source for the studied rocks is comparable to Hawaiian alkali and tholeiitic basalts, which are considered to be generated

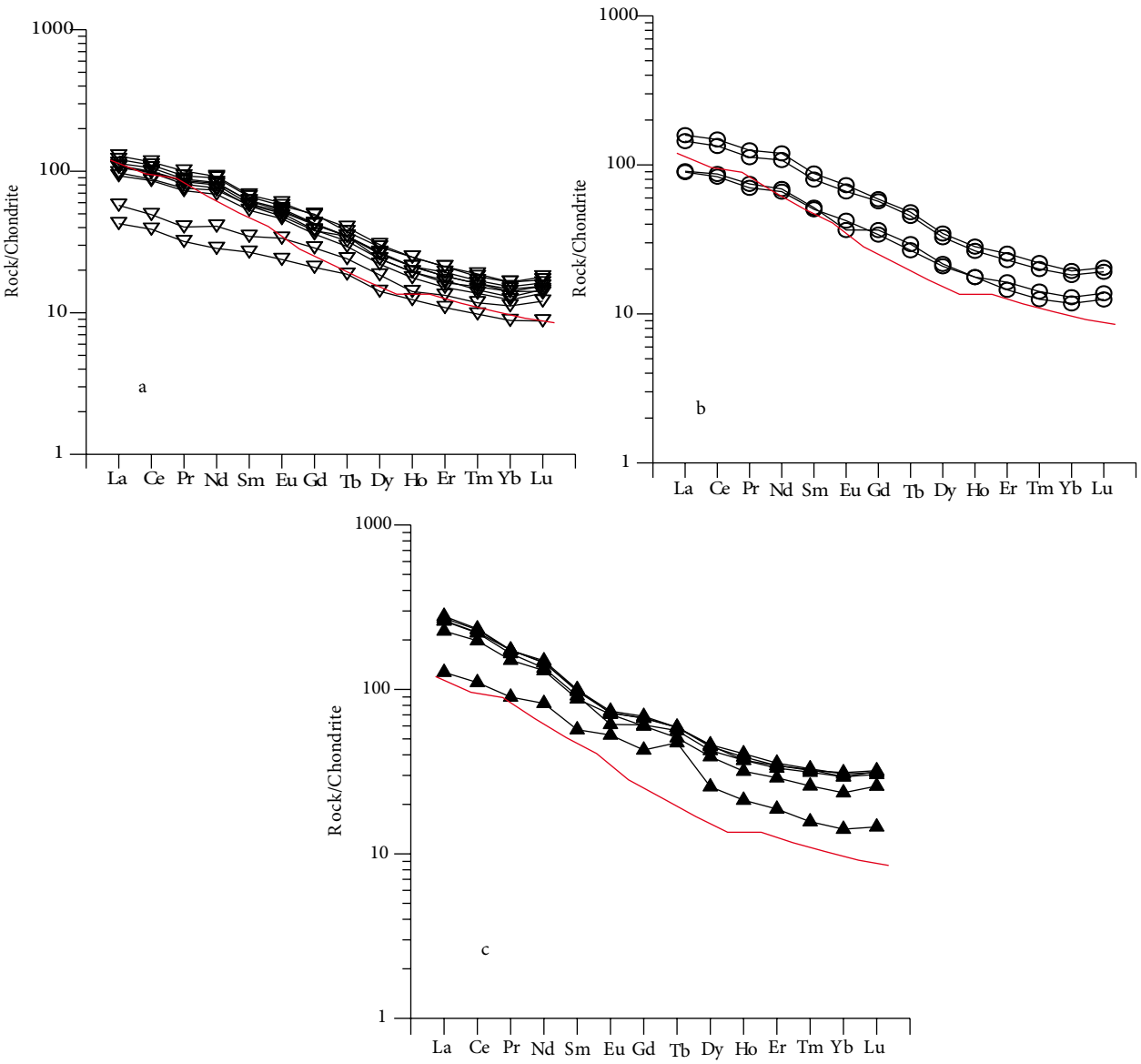

Figure 6. Chondrite-normalized REE diagrams showing parallel and inclined pattern and enrichment in LREEs similar to the OIB pattern of Sun and McDonough (1989) (red line): **(a)** gabbro, **(b)** dolerites, **(c)** diorites. Symbols as in Figure 4.

from a garnet-bearing lherzolite mantle source (Moghazi, 2003). Obiora and Charan (2010, 2011a) reported a similar range of REE ratios for intrusive and extrusive rocks in other parts of the Lower Benue rift.

The intrusive rocks have elemental ratios (La/Nb = 0.74, Th/La = 0.11, and Th/Nb = 0.07 on average) similar to the HIMU (that is, high $^{238}U/^{204}Pb$) mantle source reservoir characterized by ratios of 0.72, 0.12, and 0.09, respectively (Tatar et al., 2007). The Nb/La ratios of 1.18–1.50 for gabbro, 1.37–1.95 for dolerites, and 1.21–1.32 for diorites further indicate a HIMU mantle source reservoir in the asthenospheric mantle (Fitton et al., 1991). This is because high Nb/La ratios of approximately >1 indicate an OIB-like asthenospheric mantle source for basaltic magmas while lower ratios of approximately <0.5 indicate a lithospheric mantle source (Abdel-Fattah et al., 2004) [see Figures 7a and 7b after Menzies and Kyle (1990, as cited in Mojgan, 2008) and Fitton et al. (1991), respectively].

4.3. Crustal contamination

The Ti/Yb ratios (Table 3) are indicators of crustal contamination in basalts, since the upper and lower continental crust has low concentrations of Ti; high ratios of Ti/Yb, usually in the thousands, indicate little to no crustal contamination, whereas low ratios are inconclusive (Hart et al., 1989). The Ti/Yb ratios for the studied rocks range from 1240 to 9880 (average: 3116) for the diorite

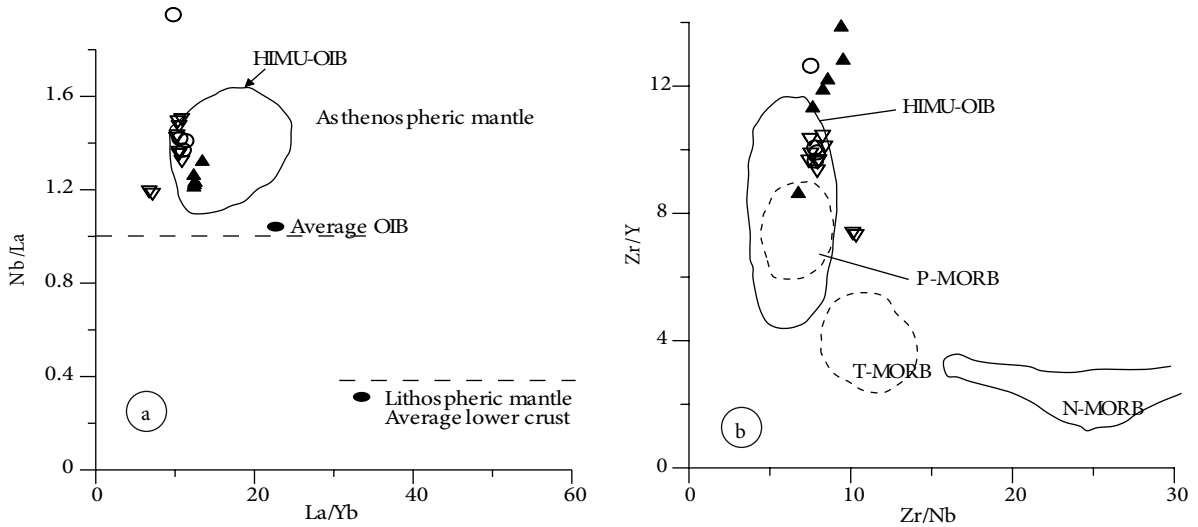

Figure 7. (a) Nb/La vs. La/Yb and **(b)** Zr/Y vs. Zr/Nb diagrams showing that the intrusive rocks plot mostly in the asthenospheric mantle with more affinity to the HIMU source of OIB. After Menzies and Kyle (1990, as cited in Mojgan, 2008) and Fitton et al. (1991), respectively. Symbols as in Figure 4.

rocks and 5425 to 13,837 (average: 9501) for the gabbro and dolerites, suggesting little or insignificant crustal contamination (Table 3).

According to Mojgan (2008), La/Nb of >1.5 indicates crustal contamination. Likewise, La/Nb ratios in the studied rocks ranged from 0.51 to 0.86 (average: 0.74), implying further evidence of less crustal contamination (Table 3).

La/Ta ratios have been used as an indicator of crustal contamination (Fitton et al., 1988; Leat et al., 1988; Thompson and Morrison, 1988). Leat et al. (1988) suggested that rocks with La/Ta ratios of <22 are derived from an asthenospheric source and have undergone little to no contamination from the continental crust or mantle lithosphere. Thompson and Morrison (1988) proposed that La/Ta ratios between 10 and 12 originate from an asthenospheric source and values of >30 indicate crustal or lithospheric contamination. The La/Ta ratios of the studied rocks range from 7.41 to 13.6, with an average of 10.9, therefore supporting an asthenospheric mantle source devoid of contamination.

Using all these parameters, it is clear that crustal contamination did not play a major role in the evolution of the studied rocks. Furthermore, insignificant crustal contamination indicates that the magma ascent may have been fast enough from the source.

4.4. Fractional crystallization and partial melting

The consistent decrease in the values of magnesium number (Mg#) of the intrusives (gabbro, 0.47 average; dolerites, 0.37 average; and diorites, 0.27 average) and the similar patterns of the gabbro, dolerites, and diorites in spider diagrams and REEs (Figure 5 and 6) show that the

Table 3. Comparison of ratios of major and trace elements in the Ishiagu igneous rocks with average contamination ratios.

	CA01A	CA01B	CA01C	CA01D	CA01E	CA01F	CA06	CA08	CA08B	CA10	CA02
La/Ta	11.67	12.47	11.58	12.1	12.37	12.69	9.64	10.7	7.41	10.7	9.63
La/Nb	0.76	0.82	0.81	0.79	0.82	0.82	0.71	0.73	0.51	0.71	0.67
Ti/Yb	2818	1485	9880	1240	1448	1825	13837	6825	12056	5425	11646
	CA03	CA03B	CA04	CA09	CA9A	CA11B	CA11C	CA12	CA13	Average	LCON*
La/Ta	11.3	10.25	10.04	13.6	12.63	9.28	10.16	10.5	10	10.9	<22
La/Nb	0.76	0.7	0.68	0.86	0.84	0.67	0.71	0.74	0.73	0.74	<1.5
Ti/Yb	7843	8877	11617	7308	7482	10413	9362	8903	11422	7585.6	>1000

*LCON = Little to no contamination values after Hart et al. (1989), Fitton et al. (1988), Leat et al. (1988), Thompson and Morrison (1988), Hawkesworth (1986), and Mojgan (2008).

basic and intermediate rocks are coeval. The differentiated product diorite has higher concentrations of the high field-strength elements (HFSEs; Zr, Nb, Y, Hf and Ta) than gabbro (early crystallized rocks), which indicates clearly that they are coeval. The $(Ta/Th)_n$ versus $(La/Sm)_n$ variation diagram of Dupuis et al. (2005) (Figure 8) shows that the major controlling factor in the evolution of the rock suite in this study was fractional crystallization, and not assimilation and fractional crystallization, with a trend of E-MORB-OIB-LCC (lower continental crust).

Experiments have shown that tholeiitic OIBs are generated in comparable degrees of partial melting to mid-ocean ridge basalt (MORB; 20%–30%), whereas alkalic OIBs may represent smaller degrees of melting (5%–15%), possibly at greater depths (Wilson, 1989). The stronger enrichment in LREEs in the alkaline rocks (gabbro, dolerite, and diorite samples) relative to the tholeiites (gabbroic stock, CA09 and CA09A) indicates that the alkaline rocks in this study have lower partial melting than the tholeiites (gabbroic stock, CA09 and CA09A). Wilson (1989) showed that degrees of magma generation and overall magma production rates are higher in areas with thinner lithosphere and lower in areas with thicker lithosphere. Therefore, tholeiitic magmas that have higher degrees of partial melting are produced in areas with thinner lithosphere in contrast with alkaline magmas, which are produced in areas with thicker lithosphere (Wilson, 1989). This is the case of Hawaii and the Canary Islands, which range from a thin to thick lithosphere at the Canary Islands off the northwestern coast of Africa in the Atlantic Ocean and have more alkaline rocks with sparse tholeiites (Wilson, 1989). This shows that the studied area of the Lower Benue rift, characterized by predominant alkaline rocks with sparse tholeiitic affinity, is probably thicker than the Hawaiian islands, which have predominant tholeiitic rather than alkaline rocks.

4.5. Tectonic setting

The predominantly alkaline and sparse tholeiitic affinity of the studied rocks may suggest an extensional tectonic setting because alkaline and tholeiitic (within-plate) rock suites are typically formed in extension regions or anorogenic settings, commonly within continental or oceanic plates such as rifting centers (Obiora and Charan, 2011a). In contrast, calc-alkaline rocks are known in subduction zones. Alkaline rocks occur in subduction zones, but towards the end of subduction, farther away from the trench, as a result of extensional stress (Nelson et al., 1995). The studied rocks reveal a within-plate tectonic setting as shown by the discrimination diagram using the less mobile HFSEs (Figures 9a). Besides, they are similar to those of the intracontinental Kenyan rift within the East African rift system as indicated on the La/10-Y/15-Nb/8 diagram of Cabanis and Lecolle (1989) (Figure 9b). On

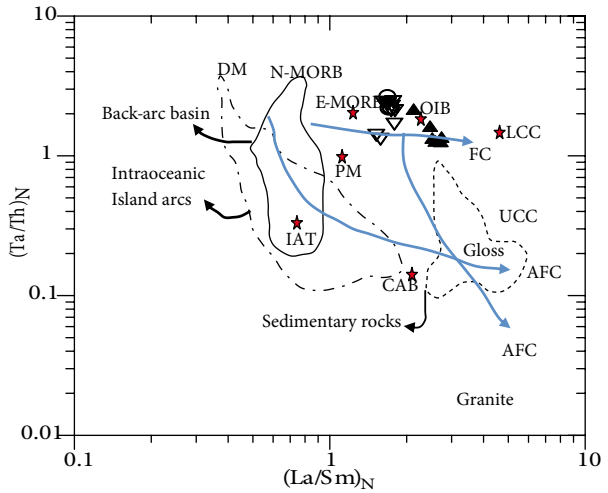

Figure 8. $(Ta/Th)_n$ versus $(La/Sm)_n$ variation diagram for the discrimination of processes involved during magma evolution. FC: fractional crystallization, DP: depleting mantle, PM: primitive mantle, LCC: lower continental crust, UCC: upper continental crust, AFC: assimilation and fractional crystallization, IAT: island arc tholeiite, CAB: calc-alkaline basalt, and Gloss: global subducting sediment (after Dupuis et al., 2005). Symbols as in Figure 4.

the discrimination diagrams of 2Nb-Zr/4-Y (Meschede, 1986) (Figure 9c), the alkaline rocks plot in the field of within-plate alkaline basalts while the 2 tholeiitic samples (gabbro, CA09 and CA09A) plot in the field of within-plate tholeiites. Although the earlier work of Farrington (1952) and Burke et al. (1971, 1972) suggested a convergent setting for the Benue rift, this work supports the views of Olade (1979), Hoque (1984), Obiora and Umeji (1995), and Obiora and Charan (2010, 2011a), who supported an extensional setting for the Benue rift.

Petrographic and geochemical study of the intrusive rocks in the study shows that the rocks are alkali gabbro, dolerites, and diorites. The gabbro and diorites occur as stocks while the dolerites occur as sills. The gabbro and dolerites consist of clinopyroxenes, plagioclase (labradorite), and altered olivine, while the diorites consist of clinopyroxene, plagioclase (andesine), and hornblende. The dolerite is differentiated from the gabbro by medium grain sizes and doleritic textures; in contrast, the gabbro has ophitic to subophitic texture. The high LOI of the intrusive rocks shows that they are relatively altered, confirmed by the alteration of clinopyroxene to large crystals of calcite and ilmenite as observed in thin section. However, critical examinations using more dependable immobile elements in discrimination diagrams, spider diagrams, and REEs clearly show that the rocks are predominantly alkaline. The ratios of La/Nb, Th/La, Th/Nb, and Nb/La suggest that the rocks may have been associated with the HIMU mantle region. The elemental ratios (La/Nb, La/Nb, and

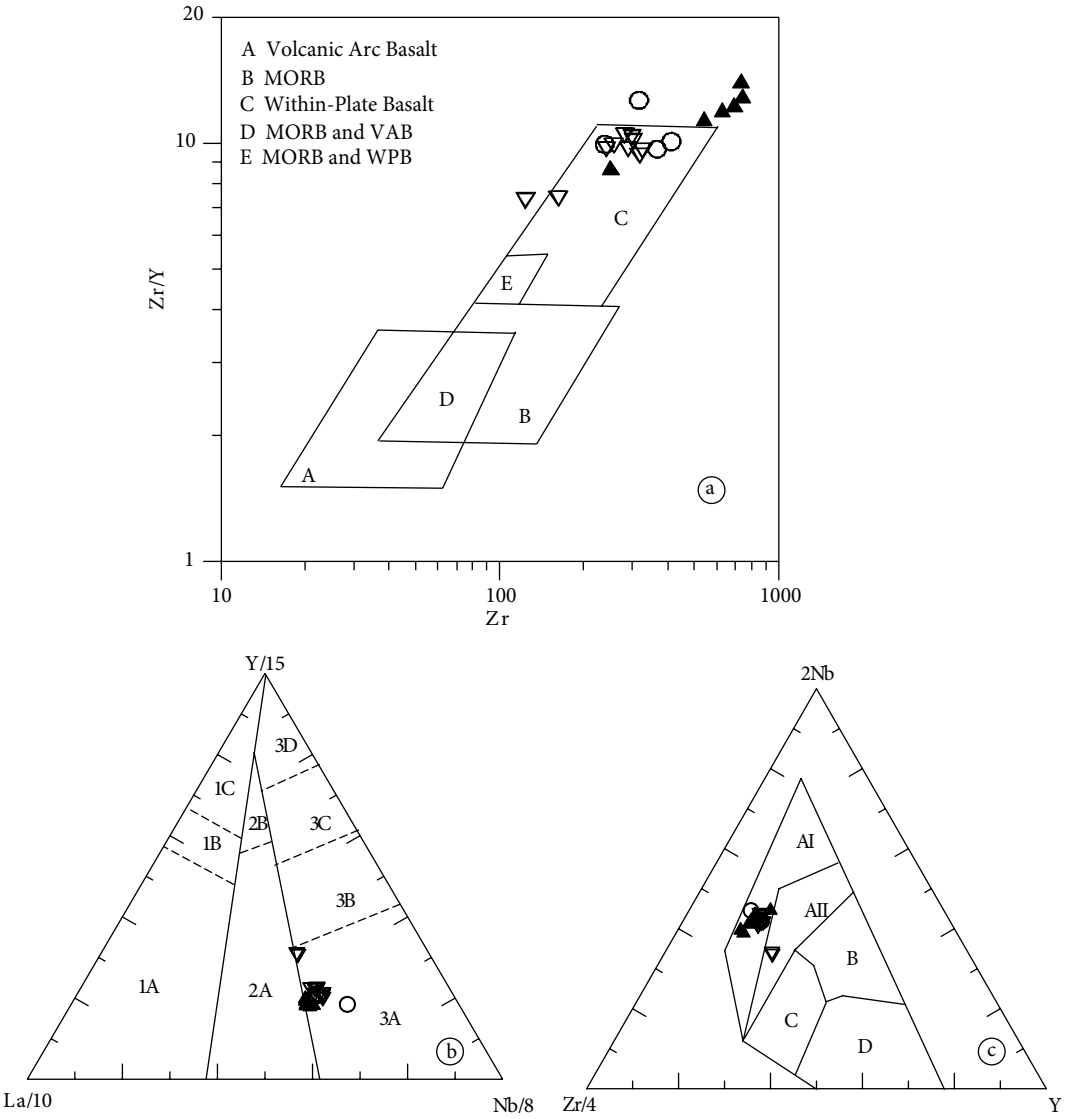

Figure 9. Plot of the Ishiagu intrusives in the tectonic discrimination diagrams. **(a)** Zr/Y versus Zr (Pearce and Norry, 1979). **(b)** Y/15-La/10-Nb/8 (Cabanis and Lecolle, 1989); field 1A = calc-alkali basalts, 1C = volcanic arc tholeiites, 1B = an area of overlap of 1A and 1C, 2A = continental basalts, 2B = back-arc basalts, 3A = alkali basalts from intracontinental rifts (e.g., Kenya rift), 3B and 3C = E-type MORB (3B: enriched, 3C: weakly enriched), 3D = N- type MORB. **(c)** Zr-Nb-Y (Meschede, 1986); AI = within-plate alkaline basalts, AII = within-plate alkaline basalts and within-plate tholeiites, B = E-type MORB, C = within-plate tholeiites and volcanic-arc basalts, D = N-type MORB and volcanic-arc basalts. Symbols as in Figure 4.

Ti/Yb) indicate that crustal contamination did not play a significant role during magma evolution. Magnesium number (Mg#), spider diagrams, and REE patterns clearly indicate that the intrusives are coeval and high ratios of $(Ta/Th)_n$ and $(La/Sm)_n$ indicate that the major controlling factor in the magma evolution is fractional crystallization. The rocks were formed in a within-plate setting of the intracontinental rift-type, similar to the Kenyan rift and Grand Canary northwestern coast of Africa in the Atlantic Ocean. The predominantly alkaline affinity, within-plate intracontinental rift (extensional) setting, and HIMU mantle source reservoir are consistent with the results obtained from igneous rocks in other parts of the Lower Benue rift.

Acknowledgments
The first author thanks Prof FI Idike (Vice-Chancellor), Prof EU Egwu (Deputy Vice-Chancellor), and the

ETF management of Ebonyi State University (EBSU), Abakaliki, Nigeria for sponsoring the geochemical analysis at the Activation Laboratories in Ontario, Canada, and also thanks Prof HN Ezeh (Dean of Students Affairs), Dr PN Nnabo (HOD, Geology Department, EBSU), and Dr OP Aghamelu for their useful contributions. We also express our regards to the management of Activation Laboratories, and especially Emmanuel Eseme, Quality Control Department, for their efforts and accuracy during the analysis.

References

Abdel-Fattah M, Abdel-Rahman AM, Nassar PE (2004). Cenozoic volcanism in the Middle East: petrogenesis of alkali basalts from northern Lebanon. Geol Mag 141: 545–563.

Benkhelil J (1986). Structure and geodynamic evolution of the intracontinental Benue Trough (Nigeria). PhD, University of Nice, France.

Benkhelil J (1987). Cretaceous deformation, magmatism and metamorphism in the Lower Benue Trough, Nigeria. Geol J 22: 467–493.

Bott MHP (1976). Mechanisms of basin subsidence – an introductory review. Tectonophysics 36: 1–4.

Burianek D, Hanzl P, Erban V, Gilikova H, Bolormaa K (2008). The early Cretaceous volcanic activity in the western part of the Gobi-Altay rift (Shiliin Nuruu, SW Mongolia). J Geosci 53: 167–180.

Burke K, Dessauvagie TFJ, Whiteman AJ (1971). Opening of the Gulf of Guinea and geophysical history of the Benue depression and Niger delta. Nature 233: 51–55.

Burke K, Dessauvagie TFJ, Whiteman AJ (1972). Geological history of the Benue Valley and adjacent areas. In: Proceedings of the Conference on African Geology, 7–14 December 1970; Ibadan, Nigeria: Department of Geology, University of Ibadan, pp. 187-205.

Cabanis B, Lecolle M (1989). La diagramme La/10-Y/15-Nb/8: un outil pour la discrimination des series volcaniques et la mise en evidence des processes de melange et/ou de contamination crustale. CR Acad Sci Ser II 309: 2023–2029 (in French).

Coulon C, Vidal P, Dupuy C, Baudin P, Poppoff M, Maluski H, Hermite D (1996). The Mesozoic to early Cenozoic magmatism of the Benue Trough (Nigeria): geochemical evidence for the involvement of the St. Helena Plume. J Petrol 37: 1341–1358.

Cratchley CR, Jones JP (1965). An interpretation of the geology and gravity anomalies of the Benue Valley, Nigeria. Overseas Geol Surv Geophys 1: 1–26.

Dupuis C, Hebert R, Dubois-Cote V, Wang CS, Li YL, Li ZJ (2005). Petrology and geochemistry of mafic rocks from mélange and flysch units adjacent to the Yarlung Zangbo Suture Zone, southern Tibet. Chem Geol 214: 287–308.

Farrington JL (1952). A preliminary description of the Nigerian lead-zinc field. Econ Geol 47: 583–608.

Fitton JG, Dunlop HM (1985). The Cameroun line West Africa and its bearing on the origin oceanic and continental alkali basalts. Earth Planet Sci Lett 72: 23–38.

Fitton JG, James D, Kempton PD, Ormerod DS, Leeman WP (1988). The role of lithospheric mantle in the generation of late Cenozoic basic magmas in the western United States. In: Cox KG, Menzies MA, editors. Oceanic and Continental Lithosphere: Similarities and Differences. J Petrol Special Volume: 331–349.

Fitton JG, James D, Leeman WP (1991). Basic magmatism associated with Late Cenozoic extension in the Western United States: compositional variations in space and time. J Geophys Res 96: 13693–13712.

Grant NL (1971). South Atlantic, Benue Trough and Gulf of Guinea Cretaceous triple junction. Geol Soc Am Bull 28: 2295–2298.

Gunthert AE, Richards HJ (1960). The geology and petrography of the pyroxene-microdiorite of Eziator Hill, Eastern Nigeria. J Schweize Mineral Petrogr Mitt Bull 40: 347–358.

Hart WK, Woldegabriel G, Walter RC, Mertzman SA (1989). Basaltic volcanism in Ethiopia: constraints on continental rifting and mantle interactions. J Geophys Res 94: 7731–7748.

Hossain MT (1981). Geochemistry and petrology of the minor intrusives between Efut Eso and Nko in the Ugep area of Cross River State, Nigeria. J Min Geol 18: 42–51.

Hoque M (1984). Pyroclastics of Lower Benue Trough of Nigeria and their tectonic implications. J Afr Earth Sci 2: 351–358.

Idowu JO, Ekweozor CM (1993). Petroleum potential of Cretaceous shales in the Upper Benue Trough, Nigeria. J Petrol Geol 21: 105–118.

Kearey P, Vine FJ (1990). Global Tectonics. London, UK: Blackwell.

Leat PT, Thompson RN, Morrison MA, Hendry GL, Dickin AP (1988). Compositionally-diverse Miocene-recent rift related magmatism in northwest Colorado: partial melting, and mixing of mafic magmas from 3 different asthenospheric and lithospheric mantle sources. J Petrol Special Volume: 351–377.

Maluski H, Coulon C, Popoff M, Baudin P (1995). 40 Ar/39 Ar chronology, petrology and geodynamic setting of Mesozoic to Early Cenozoic magmatism from the Benue Trough, Nigeria. J Geol Soc Lond 152: 311–326.

Miyashiro A (1978). Nature of alkalic volcanic rock series. Contrib Mineral Petrol 66: 91–104.

Moghazi AM (2003). Geochemistry of a Tertiary continental basalt suite, Red Sea coastal plain, Egypt: petrogenesis and characteristics of the mantle source region. Geol Mag 140: 11–21.

Mojgan S (2008). Petrology, geochemistry and mineral chemistry of extrusive alkalic rocks of the Southern Caspian Sea ophiolite, Northern Alborz, Iran: evidence of alkaline magmatism in Southern Eurasia. J Appl Sci 8: 2202–2216.

Nakamura N (1974). Determination of REE, Ba, Fe, Mg, Na and K in carbonaceous and ordinary chondrites. Geochim Cosmochim Ac 38: 757–775.

Nelson SA, Gonzalez-Caver E, Kyser TK (1995). Constraints on the origin of alkaline and calc-alkaline magmas from the Tuxtla Volcanic field, Veracruz, Mexico. Contrib Mineral Petrol 122: 191–211.

Nwachukwu SO (1972). The tectonic evolution of the southern portion of the Benue Trough, Nigeria. Geol Mag 109: 411–419.

Nwajide CS (1990). Sedimentation and paleogeography of the Central Benue Trough, Nigeria. In: Ofoegbu CO, editor. The Benue Trough: Structure and Evolution. Braunschweig, Germany: Vieweg Verlag, pp. 19–38.

Obaje NG, Ulu OK, Petters SW (1999). Biostratigraphic and geochemical controls of hydrocarbon prospects in the Benue Trough and Anambra Basin, Nigeria. NAPE Bull 14: 18–54.

Obiora SC (1994). Petrology of magmatic rocks west of Anyim river, Lower Benue Trough. MSc, University of Nigeria, Nsukka, Nigeria.

Obiora SC (2002). Evaluation of the effects of igneous bodies on the sedimentary fills of the Lower Benue rift and vice versa. PhD, University of Nigeria, Nsukka, Nigeria.

Obiora SC, Charan SN (2010). Geochemical constraints on the origin of some intrusive igneous rocks from the Lower Benue rift, Southeastern Nigeria. J Afr Earth Sci 58: 197–210.

Obiora SC, Charan SN (2011a). Tectonomagmatic origin of some volcanic and sub-volcanic rocks from the Lower Benue rift, Nigeria. Chinese J Geochem 30: 507–522.

Obiora SC, Charan SN (2011b). Geochemistry of regionally metamorphosed sedimentary rocks from the Lower Benue rift: implications for provenance and tectonic setting of the Benue rift sedimentary suite. S Afr J Geol 114: 25–40.

Obiora SC, Umeji AC (1995). Alkaline intrusive and extrusive rocks from areas west of Anyim River, Southeastern Benue Trough. J Min Geol, 31: 9–19.

Obiora SC, Umeji AC (1997). An appraisal of the use of discrimination diagrams in the tectonomagmatic classification of igneous rocks in Nigeria. In: 33rd Annual International Conference of the Nigeria Mining and Geosciences Society, Jos, Nigeria, Abstracts Volume.

Obiora SC, Umeji AC (2004). Petrographic evidence for regional burial metamorphism of the sedimentary rocks in the Lower Benue Rift. J Afr Earth Sci 38: 269–277.

Obiora SC, Umeji AC (2005). Petrography of some altered intrusives rocks from the Lower Benue Trough, Nigeria. J Min Geol 41: 1–8.

Ofoegbu CO, Amajor LC (1987). A geochemical comparison of the pyroclastic rocks from the Abakaliki and Ezillo, Southern Benue Trough. Nigeria. J Min Geol 23: 45–52.

Olade MA (1975). Evolution of Nigeria's Benue Trough (Aulacogen): a tectonic model. Geol Mag 112: 575–581.

Olade MA (1978). Early Cretaceous basalt volcanism and initial continental rifting in Benue Trough, Nigeria. Nature 273: 458–456.

Olade MA (1979). The Abakaliki pyroclastics of the Southern Benue Trough, Nigeria; their petrology and tectonic significance. J Min Geol 16: 17–24.

Pearce JA (1982). Trace elements characteristics of lavas from destructive plate boundaries. In: Thorpe RS, editor. Andesites. Chichester, UK: Wiley, pp. 525–548.

Pearce JA (1996). A user's guide to basalt discrimination diagrams. In: Wyman DA, editor. Trace Element Geochemistry of Volcanic Rocks: Applications for massive Sulphide Exploration. Geol Assoc Can 12: 79–113.

Pearce JA, Cann JR (1973). Tectonic setting of basic volcanic rocks determined using trace element analyses. Earth Planet Sci Lett 19: 290–300.

Pearce JA, Norry MJ (1979). Petrogenetic implications of Ti, Zr, Y and Nb variations in volcanic rocks. Contrib Mineral Petrol 69: 33–47.

Petters SW (1978). Idle Cretaceous paleoenvironments and biostratigraphy of the Benue Trough, Nigeria. Geol Soc Am Bull 89: 151–154.

Rollinson HR (1993). Using Geochemical Data: Evaluation, Presentation, Interpretation. London, UK: Longman.

Roy P, Balaram V, Kumar A, Satyanarayanan M, Rao TG (2007). New REE and trace data on two kimberlitic reference materials by ICP–MS. Geostand Geoanal Res 31: 261–273.

Sayıt K, Göncüoglu MC (2009). Geochemistry of mafic rocks of the Karakaya complex, Turkey: evidence for plume-involvement in the Palaeotethyan extensional regime during the Middle and Late Triassic. J Earth Sci 98: 367–385.

Sun SS, McDonough WF (1989). Chemical and isotopic systematic of oceanic basalts: implications for mantle composition and processes. Spec Publ Geol Soc 42: 313–345.

Thompson RN (1982). British Tertiary volcanic province. Scottish J Geol 18: 49–67.

Thompson RN, Morrison MA (1988). Asthenospheric and lower lithospheric mantle contributions to continental extension magmatism: an example from the British Tertiary Province. J Chem Geol 68: 1–15.

Umeji AC (1985). Aspects of some the volcanic and sub-volcanic rocks in the Lower Trough. J Min Geol 22: 199–204.

Umeji AC (2000). Evolution of the Abakaliki and the Anambra basins, Southeastern Nigeria. A Report Submitted to the Shell Petroleum Development Company Nigeria Limited.

Uzuakpunwa AB (1974). The Abakaliki pyroclastics, eastern Nigeria: new age and tectonic implications. Geol Mag 111: 761–769.

Wilson M (1989). Igneous Petrogenesis. London, UK: Unwin Hyman.

Wilson RC, Bain AD (1928). The Nigerian coal fields. Section II. Parts of Onitsha and Owerri Provinces. With an Appendix by L.F. Spath on the Albian Ammonoidea of Nigeria. Geological Survey of Nigeria Bull 12: 54.

Winchester JA, Floyd PA (1977). Geochemical discrimination of different magma series and their differentiation products using immobile elements. J Chem Geol 20: 325–343.